論文 / 著書情報
Article / Book Information

論題(和文)	
Title(English)	Measurement of Porosity in Three-way Catalyst Particles Membrane Filter using Electron Microscopy Image Analysis
著者(和文)	Ko Ko Phyo Zin, SUTEERAPONGPUN Teerapat, 花村 克悟
Authors(English)	Koko Phyozin, Teerapat Suteerapongpun, Katsunori Hanamura
出典(和文)	, Vol. 14, No. 1, pp. 27 - 34
Citation(English)	International Journal of Automotive Engineering, Vol. 14, No. 1, pp. 27 - 34
発行日 / Pub. date	2023, 1

Koko Phyozin et al. / International Journal of Automotive Engineering
Vol.14, No.1(2023)
Research Paper
20234117

Measurement of Porosity in Three-way Catalyst Particles Membrane Filter using Electron Microscopy Image Analysis

Koko Phyozin [1)] Teerapat Suteerapongpun [1)] Katsunori Hanamura [1)]

1) Department of Mechanical Engineering, School of Engineering, Tokyo Institute of Technology, Japan
(E-mail: koko.p.aa@m.titech.ac.jp)

Received on October 27, 2022

ABSTRACT: A membrane filter was fabricated using gas dispersant micro-sized Three-way Catalyst (TWC) particles on the conventional filter substrate. The porosity of the cross-sectional area of the TWC-membrane was measured through electron microscopy image processing technique. In the membrane manufacturing process, a parametric study was conducted by comparing three mean particle sizes under three superficial velocities. According to high resolution electron micrographs, the cross-sectional view of a single TWC-particle was revealed as a homogeneously agglomerated particle. The porosity of the cross-sectional area of the membrane was measured as approximately 64.4% with a slight difference about 3% depending on varying mean particle sizes and superficial velocities.

KEY WORDS: Membrane filter, Three-way Catalyst, Porosity, Electron Microscopy

1. Introduction

Particulate filters have been used for many decades as a post-combustion exhaust gas control system for the particulate matters emitted from internal combustion engines. At present, the wall flow ceramic honeycomb diesel particulate filter (DPF) can achieve over 90% filtration efficiency[1][2]. According to stringent emission regulations, gasoline direct injection (GDI) engines must equip with gasoline particulate filters (GPF) by following the previous DPF technology. By installing GPF in gasoline engines, not only particulate mass PM but also particle number PN can be significantly reduced, which will meet with the current emission regulation[3][4]. Compared to port fuel injection PFI engines, gasoline direct injection engines can obtain greater engine output power, less fuel consumption and higher thermal efficiency but it emits significantly large number of particulates because of direct fuel injection inside combustion chamber through nozzle. Besides, GDI engine emits finer particulates, but larger number of particulates compared to diesel engines[5][6][7].

Three-way catalytic (TWC) converters were applied for many decades in gasoline engines in order to oxidize exhaust gas pollutants such as carbon monoxide (CO), unburnt hydrocarbons (HCs) and reduce nitrogen oxides (NO_x) simultaneously. The conventional TWC monolith is mainly composed of ceria-zirconia mixed metal oxides catalyst as oxygen storage materials due to its promising redox performance in catalytic reaction[8][9]. In the past, three-way catalyst was wash-coated in gasoline particulate filters in order to obtain the efficient removal of both combustion derived soot particles and gaseous components. On the other hand, there is a trade-off relationship between gas conversion efficiency and engine back pressure. The contribution of TWC in GPF is also known as catalyzed gasoline particulate filter[10][11]. According to the previous works from our laboratory, various catalyst components were fabricated as a membrane on a conventional particulate filter substrate which can result significant effect on soot filtration and oxidation phenomena. A diesel particulate membrane filter made of zeolite mixing with K, Na and Cs catalyst advanced soot oxidation kinetics compared to the conventional DPF. Because of the catalytic performance of mixed zeolite catalyst membrane, the activation energy needed to oxidize the soot cake layer during regeneration was reduced to about 20%[12]. In an internal combustion engine, back pressure caused by particulate filters is the accumulation of soot along the pores of the substrate and the formation of soot cake layer. By using time-lapse visualization method, pressure-drop characteristics (S-shape) in the conventional DPF can be clearly identified into three major stages as bridging, surface pore filtration and cake layer formation. In the DPF, the drastic increase in pressure drop is the result of soot accumulation in the surface pores[13][14]. Manufacturing membrane particulate filter on the conventional DPF is one of the solutions to lessen the substantial pressure drop increase caused by the surface pore filtration stage. In fact, when a membrane covers the entrance of the surface pore, soot is deposited only in the small pores of the membrane. As a result, high gradient of pressure drop increase caused by the surface pore filtration stage was significantly reduced. By fabricating a catalyst membrane on the conventional DPF, not only total increase in pressure drop was lower but also initial soot filtration efficiency became higher[15]. Recently, a catalyst membrane made of nano- catalyst particles such as Pt-Pd and Ag-Pd fabricated on an alumina supporter showed lower soot oxidation temperature and CO emission can be reduced[16][17].

In the current study, a TWC-particles membrane filter was manufactured on a bare particulate filter substrate and the porosity of the membrane was measured using an electron microscopy image analysis. A porosity measurement method which was measured on the cross-sectional view of TWC-membrane layer was introduced. Parametric study was conducted by introducing three different agglomerated TWC-particle sizes under three superficial velocity conditions.

2. Experimental Method

A miniature particulate filter sample composed of 7x7 channels with a precise dimension of 10 mm^3 was extracted from a conventional full-size silicon carbide (Si-C) particulate filter substrate. High temperature resistance ceramic paste was used to plug at the end of the channels alternately. After plugging the alternate channels, the total filtration area of the inlet channels was calculated as about 829.8 mm^2. Then, the plugged sample was placed inside a stainless-steel holder. The top surface of the sample was polished to achieve up to a mirror-like top surface by using various abrasive discs (P600 to P4000). The top surface was covered by a quartz glass plate and clamped with bolts and nuts. As a result, there was no gas leakage from the cross-sectional top surface when the working gas was introduced from the upstream side channels of the sample.

The schematic diagram of the experimental setup of fabricating membrane filter on a conventional filter substrate is described in Fig.1. To fabricate the TWC-particles membrane, a three-way catalyst slurry package composed of 20 wt% of TWC-particles was used. In the slurry, the aggregated primary particulates (approximately 200 nm in average diameter) were heterogeneously mixed with distilled water as shown in Fig.2. The catalyst slurry was placed in an acrylic tube and atomized into small droplets (approximately 5-10 microns) using an ultrasonic atomizer (60 Hz frequency). The carrier gas (Nitrogen) was introduced into the inlet of the acrylic tube under a flow rate of 50 mL/min. Gas dispersant particles in the form of water droplets were carried through the outlet of the tube. Dilution gas was introduced at the entrance of an evaporator to obtain the desired superficial velocity and a lower humidity than a dew point even at the room temperature. Then, the nitrogen dispersant water droplet particles were passed through the evaporator which was constantly preheated at 280°C by using a ribbon heater. As a result, an agglomerated TWC-particle was manufactured by vaporizing the water droplet particle. Finally, the agglomerated nitrogen dispersant particles were deposited as a membrane layer on the bare Si-C particulate filter substrate. The thickness of the TWC-particles membrane on the substrate was about 40 microns. According to the process of atomization, the concentration of TWC-particulates in the slurry varies the sizes of agglomerated particle. Therefore, the sizes of agglomerated TWC-particles were controlled by diluting the original 20 wt% TWC particulates slurry using distilled water. Moreover, the chemical composition of the slurry was much the same as the composition of commercial TWC monolith converter as described in Fig.3.

During fabricating the membrane, the pressure drop increase according to the deposited weight was intermittently measured. The pressure drop was measured using a high-precision digital manometer by tap-fixing at the upstream and the downstream sides of the sample, P_1 and P_2, respectively, as shown in Fig.1, while a digital micro-weighing scale was used to measure the deposited weight. In this case, the weight of the intermittently-fabricated sample with the holder and the quartz glass plate was measured at each interval of deposition after the bolts and nuts clamping setup was removed.

Here, to investigate the pressure-drop increase with respect to deposited weight of the TWC-particles, membrane fabrication process was conducted in a humidity-controlled gloves box to remove an erratic moisture concentration in the sample[18]. Relative humidity in the gloves box was constantly maintained at 30% with only ±2% discrepancy during the whole membrane fabrication process.

In the manufacturing process, a low superficial velocity is preferable to deposit the agglomerated TWC-particles just around the entrance of the surface pores of the substrate according to the experience of the previous works using time-lapse visualization[13][14][15]. However, since a superficial velocity such as a few milli- meters per second is close to a falling velocity caused

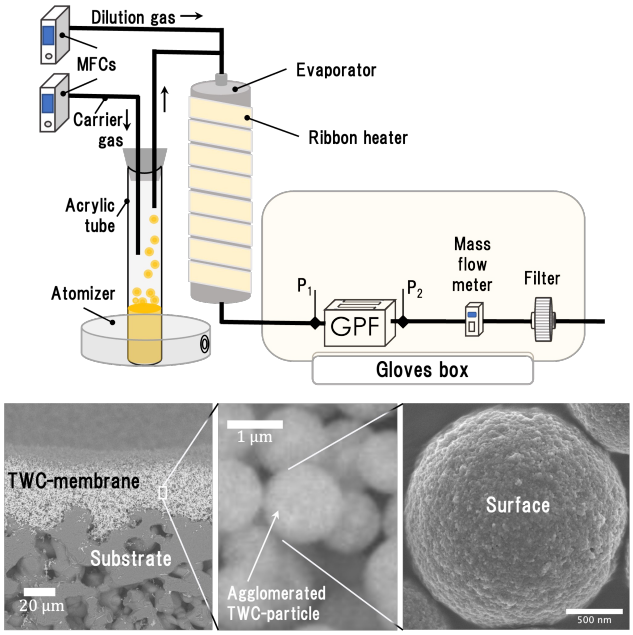

Fig. 1 Experimental setup of manufacturing TWC-particles membrane on the conventional filter substrate

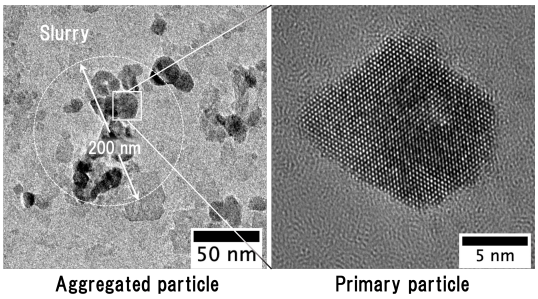

Fig. 2 TEM images of aggregated particulate (left) and primary particulate (right) in the catalyst slurry

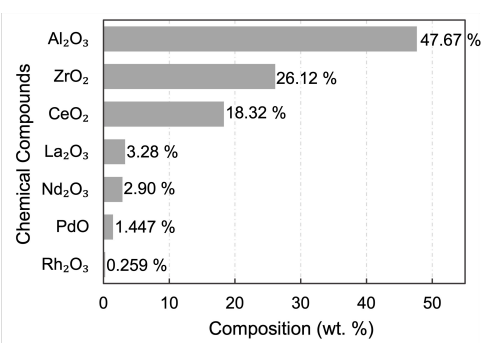

Fig. 3 Chemical composition of the catalyst slurry

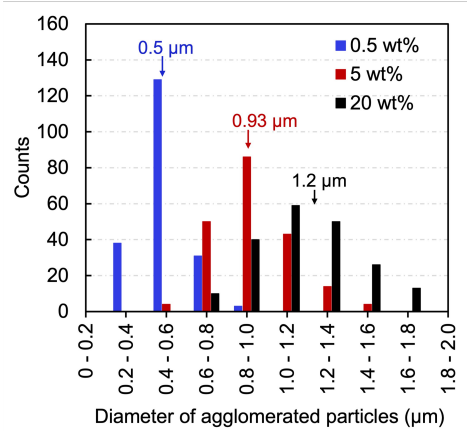

Fig. 4 Agglomerated TWC-particle size distribution under different particulate concentration in the slurry

by a gravitational force, it is not controllable to manufacture a uniform particle layer. In the current study, the superficial velocity of 5 mm/s is fixed as the minimum one to confirm the convective flowing deposition.

To measure the porosity of the cross-sectional TWC-particles membrane layer the fabricated sample was sintered at 800 degrees C for 4 hours before it was infiltrated by an epoxy resin. The resin gradually flows inward through the membrane to avoid the membrane deformation caused by infiltration. After the resin was was steadily poured from the bottom part of the sample and thoroughly embed, the sample was placed under a vacuum pressure (-50 kPa) for 15 minutes to penetrate the resin evenly until the deeper area of the pores. The ramping rate of vacuum pressure may affect the deterioration of the porous structure of the membrane. Therefore, some trials have been conducted under different pressure ramping conditions such as (i) rapidly increase the vacuum pressure from atmospheric pressure to -50 kPa, varying pressure ramping rates as well as (ii) -2 kPa/min and (iii) -10 kPa/min. It was found that there were no differences in porous structure of the TWC-membrane although various ramping rates were introduced. In fact, the sintered TWC particles can resist to infiltrate the epoxy resin under the vacuum pressure. The resin infiltrated sample was cured in the atmosphere for 24 hours. Finally, the sample was polished under water polishing to visualize the cross-sectional view of TWC-membrane layer. Due to less electron conductivity property of epoxy resin under scanning electron microscopy observation, cross-sectional top surface was transparent through deeper area. Therefore, Gold (Au) sputtering process was essential to utilize to observe the cross-sectional surface. The top surface of the sample was coated with a 50 nm Au-layer which can provide higher electron conductivity at the cross-sectional top surface.

3. Results and Disucssion

Figure 4 shows particle size distribution of agglomerated TWC-particles. By introducing different TWC-particulate concentration such as 0.5, 5 and 20 wt.% in the water-slurry, different sizes of agglomerate particles can be manufactured. As a result, a wider range of particle size distribution (ranging between 0.9 to 1.5 µm) were produced in 20 wt.% condition while a small range of particles (0.4 to 0.7 µm) were produced in 0.5 wt.% condition. Arithmetic mean diameters of the particles (measured as 200 particles in total) in each 20, 5 and 0.5 wt.% concentration were measured as 0.50, 0.93 and 1.2 µm respectively.

Figure 5 shows the effect of TWC-particle sizes of 0.5, 0.93 and 1.2 µm on the pressure drop increase and its increase rate under the condition of superficial velocity of 5 mm/s. The pressure drop is drastically increased with respect to the accumulated weight up to an inflection point whereas the bridge formation by the TWC-particles is completed[13][14]. During the bridge formation process from the beginning of deposition, the pressure drop increase rates for all TWC-particle sizes are much the same due to the same mechanism of the bridge growth[14]. Then, the larger TWC-particle size the faster the surface pores are closed by the bridge made of TWC-particles. As a result, a slightly smaller amount of TWC-particles is used to reach the inflection point in the case of larger TWC-particles. Moreover, during both surface pore and cake layer accumulation, the pressure drop for the larger TWC-particle size is lower than that of smaller particle sizes. Because at the same accumulated weight of TWC-particles, the particle number might become smaller and the pore size might become larger in the case of larger particle size. Here, when the Stokes' force around a single

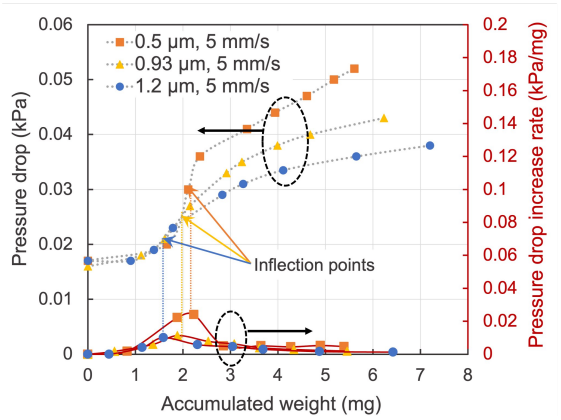

Fig. 5 Pressure drop increase in fabricating TWC-membrane by introducing different particle sizes (0.5, 0.93 and 1.2 µm) under the same superficial velocity of 5 mm/s

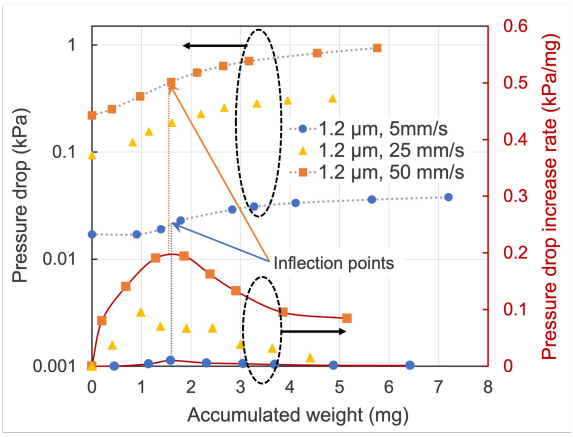

Fig. 6 Pressure drop increase in fabricating TWC-membrane by introducing same particle size of 1.2 µm under different superficial velocity conditions

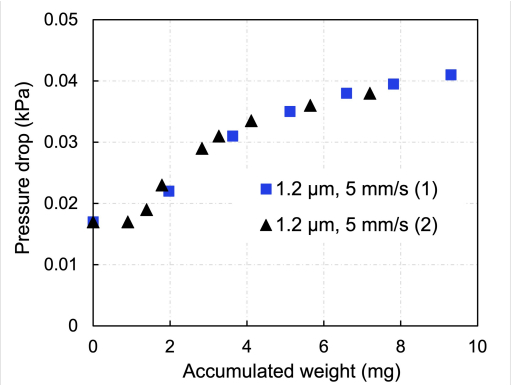

Fig. 7 Pressure drop increase in fabricating TWC-membrane by introducing same particle size of 1.2 μm under the same superficial velocity of 5 mm/s

TWC-particle is assumed, the total pressure drop depends on the product of the particle number and the Stokes' force, while many straight capillary pores are assumed in the TWC-particles membrane structure, the total pressure is proportional to the inverse of the square of pore diameter.

Figure 6 shows the effect of the superficial velocities of 5, 25 and 50 mm/s on the pressure drop increase under the condition of the TWC-particle size of 1.2 μm. The initial pressure drop increases almost in proportion to the superficial velocity. However, during both bridge formation and surface pore accumulation processes, the pressure drop increase rate is not proportional to the superficial velocity since some TWC-particles reach the deep area of substrate pores and complete the bridge formation at the deeper location in the case of the higher superficial velocity[15]. Aa a result, although much the same amounts of TWC-particles are used (except for the case of the superficial velocity of 25 mm/s) to reach the inflection points as mentioned above, the pressure drop increase becomes higher than the proportional increase. On the other hand, during the cake layer accumulation, the pressure drop increase rate increases almost in proportion to the superficial velocity.

In the case of the superficial velocity of 25 mm/s, the initial pressure drop without deposition of TWC particles reaches the almost proportional value with increase in superficial velocity from 5 to 25 mm/s. However, during bridge formation and surface pore deposition, the pressure drop does not increase as expected, that is, the pressure drop increase rate (right hand side vertical axis) goes down around the accumulated weight of 1.4 mg and then keeps at constant unlike the cases of 5 and 50 mm/s. This is because there is some flowing-gas leakage which is caused by the disassembly of fixing setup during each interval of deposited weight measurement. It is confirmed that in the case of almost-perfect assembly, there is a high reproducibility as shown in Fig.7, in which the first measured pressure drop increase (1) are much the same as the second one (2) with respect to the accumulated TWC-particles weight.

Figures 8(a) ~ 8(f) display SEM micrographs of the cross-sectional views of TWC-particles membranes fabricated on a conventional filter substrate for all experimental conditions. Although the bridge location cannot be determined clearly, the TWC-particles are deposited only around the entrance of the surface pore of the substrate filter in the case of particle size of 0.5 μm under the condition of superficial velocity of 5 mm/s as shown in Fig.8(a). With increasing particle-size to 0.93 and 1.2 μm, the TWC-particles reach slightly the deeper area of the surface pores and make the bridge at the deeper location as shown in Figs.8(b) and 8(c) due to the greater inertial force of the larger particles, but the bridge formation was not very deep. On the other hand, the number of TWC-particles for closing the surface pores decreases with increasing particle-size if the average surface pore diameters are the same in Figs.8(a), 8(b) and 8(c).

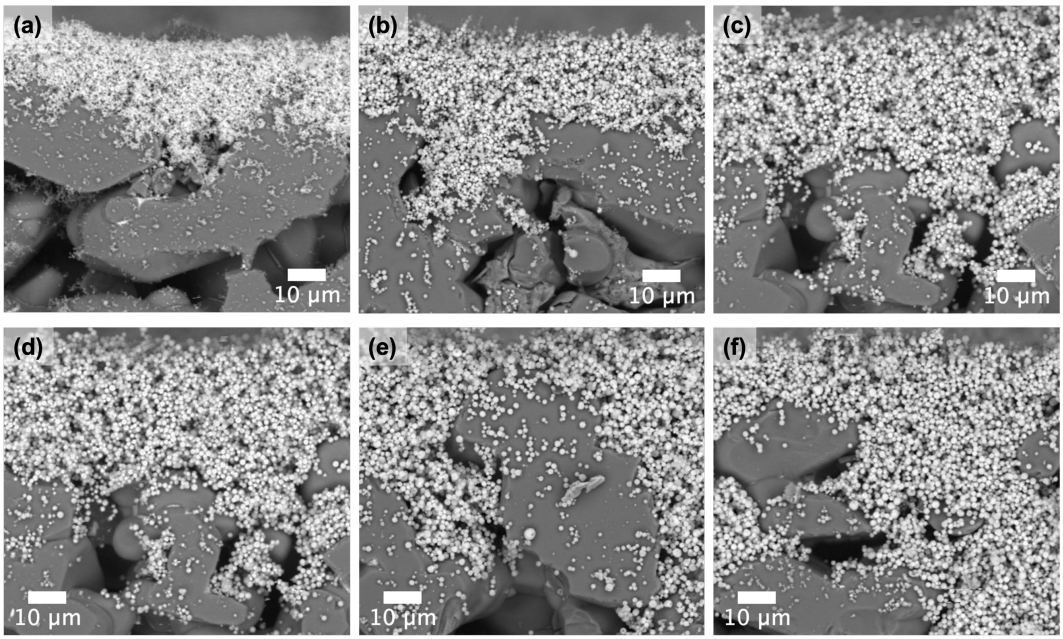

Fig. 8 SEM micrographs of cross-sectional view of TWC-particles membrane fabricating by using different particle sizes (a) 0.50 μm (b) 0.93 μm and (c) 1.2 μm under a same superficial velocity of 5 mm/s, and same particle size of 1.2 μm under different superficial velocities (d) 5 mm/s (e) 25 mm/s and (f) 50 mm/s

Using the same TWC-particle size of 1.2 μm, with increasing superficial velocity from 5 mm/s to 25 mm/s and 50 mm/s, the penetration depth of TWC-particles becomes deeper as shown in Figs.8(d), 8(e) and 8(f). Because a trapping possibility by Van der Waals force will be reduced due to a high momentum of TWC-particles as the velocity becomes higher. The accumulation of TWC-particles from the deep location to the entrance of surface pores causes a high pressure drop increase during the surface pore accumulation process as mentioned in Fig.6.

To measure the porosity of the TWC-membrane, the resin infiltrated cross-sectional area was observed through SEM and FE-SEM as described in Figs.9(a) and 9(b), respectively, at the same location. Here, the back-scattered electron (BSE) image is used in the case of the SEM. Although the borderlines between the cross-sectional TWC-particles and the resin are not clear enough for image processing analysis, the SEM images are useful to specify the location even if a whole particle is completely immersed as shown in Fig.9(a). On the other hand, using the secondary electron in the FE-SEM, the borderlines of cross-sectional TWC-particles separated from the resin surface can be observed clearly as shown in Fig.9(b), where the image of immersed particles are completely disappeared.

Figures 10(a), and 10(b) show highly-magnified FE-SEM images of the cross-sectional areas depicted by the dotted, the dashed and the solid lines in the same image as Fig.9(b). It is clarified that the primary TWC particulates are homogeneously agglomerated in the whole area of the single TWC-particle from the surface to the center because the morphology is similar to that of the spherical surface as shown in Fig.1. The borderlines of the cross-sectional area of TWC-particles can be observed clearly and are almost absolute circular shapes as shown in Fig.10(a). However, some cross-sectional areas are not absolutely circular because of partial separation of a thin resin film covering the spherical surface of the TWC-particle. Moreover, a thin resin-covered portion can be observed as the cross-sectional area due to electron penetration. Therefore, to measure the true cross-sectional TWC-particle area, an inscribed circle area should be used as the cross-sectional area of a single TWC-particle. In addition, during water polishing, it was inevitable that some particles can be released and remained as lacks on the resin surface as shown in Fig.10(b). Therefore, the inscribed circle lack areas should be counted as cross-sectional TWC-particle areas in the porosity measurement.

Figures 11 and 12 show processes of image analysis using an "Image-J" image processing program to obtain the porosity. Figures 11(a), 11(b) and 11(c) are for the TWC-particle sizes of 1.2, 0.93 and 0.5 μm, respectively, under the condition of the superficial velocity of 0.5 mm/s. Figures 12(a), 12(b) and 12(c) are for the superficial velocities of 0.5, 25 and 50 mm/s, respectively, under the condition of the particle size of 1.2 μm.

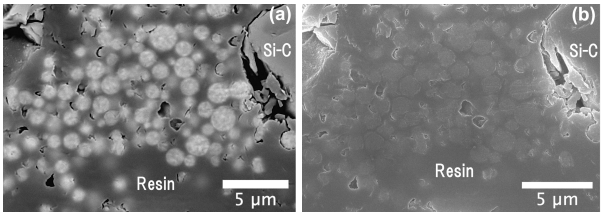

Fig. 9 Cross-sectional view of resin-inflitrated TWC-membrane through (a) SEM (b) FE-SEM

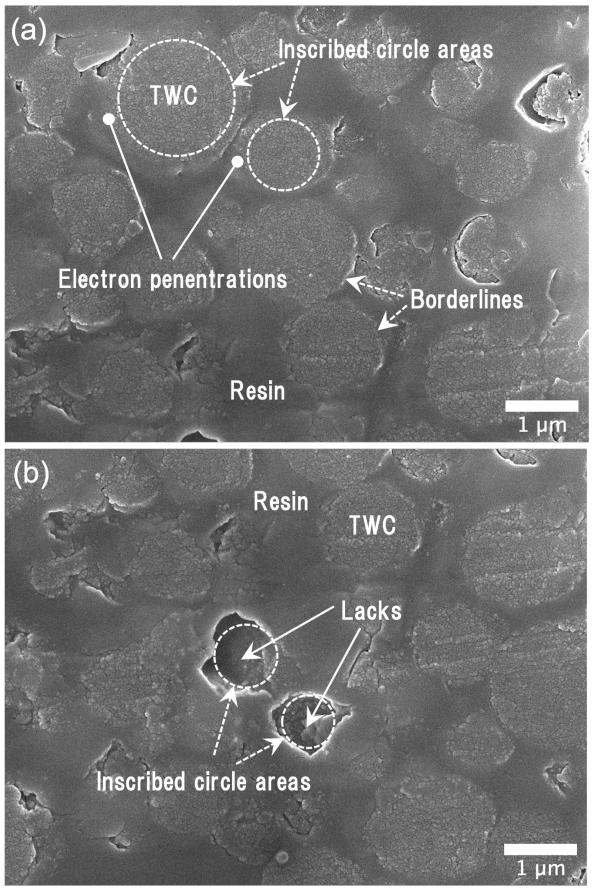

Fig. 10 Highly-magnified FE-SEM images of cross-sectional view of resin infiltrated TWC-particles membrane

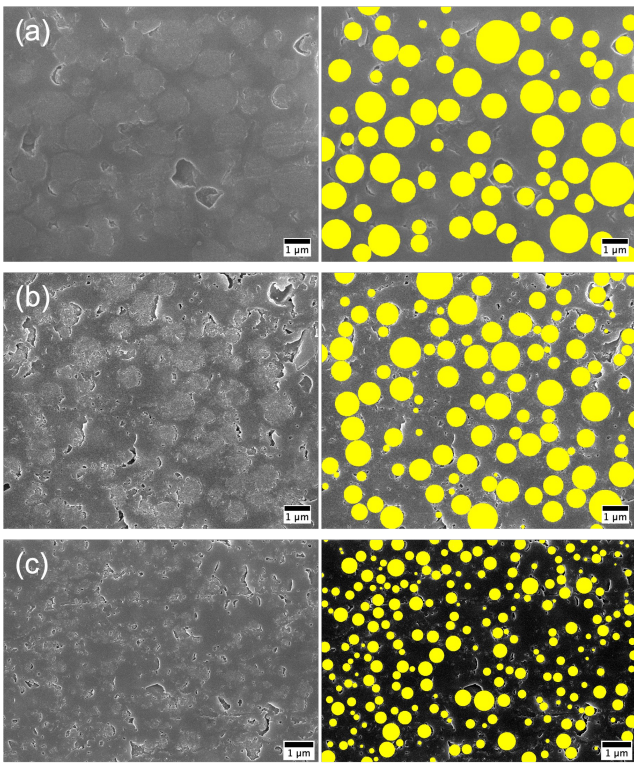

Fig. 11 Image processing analysis of porosity measurement comparing different TWC-particle sizes (a) 1.2 μm (b) 0.93 μm (c) 0.50 μm under the superficial velocity of 5 mm/s

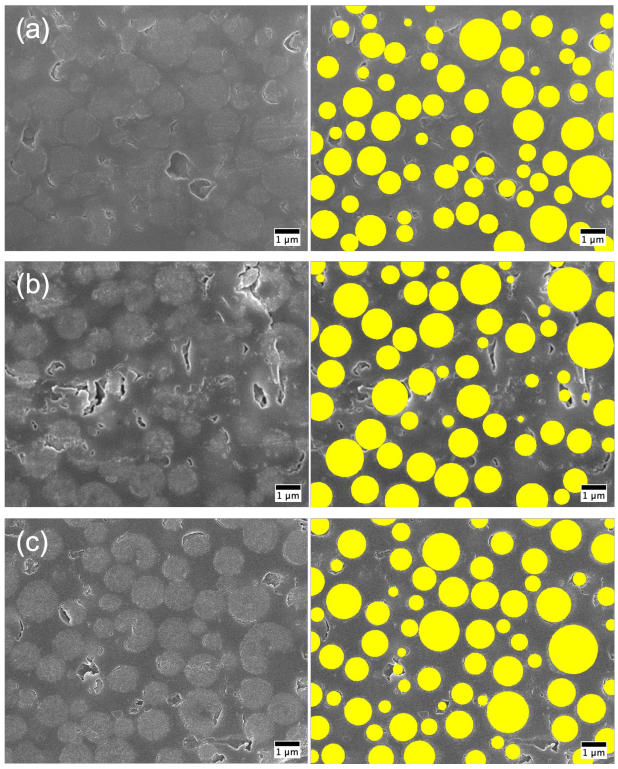

Fig. 12 Image processing analysis of porosity measurement comparing under the TWC-particle size of 1.2 μm under different superficial velocities (a) 5 mm/s (b) 25 mm/s (c) 50 mm/s

The total cross-sectional area of the TWC-particles is expressed as a summation of total depicted inscribed circle areas as shown in each right hand side image in Figs.11 and 12. The porosity, ∅ is defined as the ratio of the total cross-sectional area of the TWC-particles and total measured square-area as described as follows.

$$\phi = \left(1 - \frac{Total\ area\ of\ TWC\ particles}{Measured\ area}\right) \quad (1)$$

The measurement process was repeated up to three times for each sample to express the uncertainty of manually depicting the cross-sectional area. The average porosities for three particle sizes and three superficial velocities conditions are summarized in Table 1. The average porosity of TWC-particles membrane fabricated with the mean diameter of 1.2 μm under the superficial velocity of 5 mm/s was measured as approximately 64.4 %. With decreasing particle-size to 0.93 and 0.5 μm, the porosity increases slightly. In the current range of TWC-particle size, since impaction and interception phenomena are dominant as the particle deposition mechanism, much the same porosities are obtained. Only small increase in porosity with decreasing size might come from a decrease in inertial force of the TWC-particle. In the previous work[15], the porosity of 94.3 % was obtained in the case of alumina-particle with the mean diameter of 0.355 μm due to slight contribution of random walk (also known as Brownian motion). On the other hand, the porosity decreases slightly with increasing superficial velocity from 5 mm/s to 25 and 50 mm/s under the condition of TWC-particle size of 1.2 μm. Since with increasing superficial velocity, the momentum of TWC-particle increases, the TWC-particles might be deposited slight-densely.

The permeability of the TWC-particles membrane filter can be estimated using a Kuwabara's model[19] using the porosity, ∅, and the diameter of the TWC-particle, *d*, as described as follows:

$$k = \frac{d^2}{18\,(1-\phi)}\left(1 - \frac{9}{5}\,(1-\phi)^{\frac{1}{3}} + (1-\phi) - \frac{1}{5}(1-\phi)^2\right) \quad (2)$$

The estimated permeability of the TWC-particles membrane filter for all experimental conditions are also described in Table 1. In this model, the permeability depends directly on the square of particle diameter. As a result, the permeability is dominantly increased with TWC-particle size as 0.27 x 10^{-14} (0.5 μm), 0.86 x 10^{-14} (0.93 μm) and 1.23 x 10^{-14} m^2 (1.2 μm) since there is only small difference of porosity.

This high permeability will affect the pressure drop increase during bridge formation and surface pore deposition. As shown in Fig.13, the bridge formation starts from deposition of TWC-particles on the surface of the Si-C substrate around the first narrow area from the entrance of the surface pore. At this term, most of flowing-gas as depicted by red arrows passes through the center hole since the pressure drop for flowing through the hole is smaller than that of flowing through the TWC-particles membrane. Therefore, the flying TWC-particles are trapped at the tip of the bridge made of TWC-particles. Then, the TWC-particles bridge makes a growth towards the center of the substrate pore. During the

Table 1 Porosity and permeability of TWC-membrane

Mean diameter of TWC-particle (um)		Porosity (%)	Permeability (m^2)
Superficial velocity = 5 mm/s	0.5	67.04 (±1.17)	0.27 x10^{-14}
	0.93	66.83 (±1.64)	0.86 x10^{-14}
	1.2	64.40 (±1.44)	1.23 x10^{-14}
Superficial velocity (mm/s)		Porosity (%)	Permeability (m^2)
Mean diameter of TWC-particle = 1.2 um	5	64.40 (±1.44)	1.23 x10^{-14}
	25	63.85 (±3.32)	1.18 x10^{-14}
	50	61.75 (±1.15)	0.98 x10^{-14}

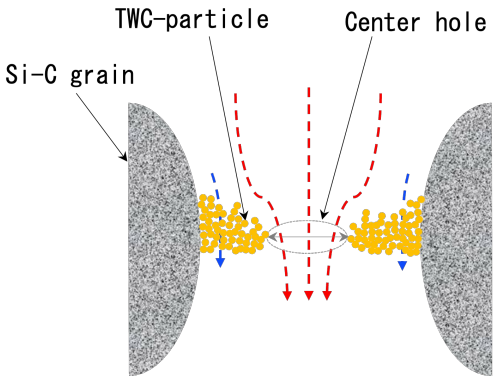

Fig. 13 Schematic image of TWC-particles deposition

bridge formation, the center hole becomes smaller and smaller. Here, when the permeability of the TWC-particles membrane is low, there is no flowing through the membrane until the hole is closed, i.e., completion of bridge formation, which contributes to a high pressure drop increase around the inflection point. On the other hand, in the case of the high permeability, it is expected that there is some gas flowing through the membrane as depicted by blue arrows from quite a while before the hole is closed. As a result, the pressure drop at the inflection point for the 1.2 μm size as shown in Fig.5 is low compared with those for 0.5 and 0.93 μm sizes, moreover, the inflection point might not be necessarily coincident with the completion of bridge formation.

On the other hand, under the condition of the same TWC-particle diameter of 1.2 μm, a 2.7% difference of porosity between 64.4 and 61.75 % leads to almost 25 % difference of permeability as 1.23 x 10^{-14} and 0.98 x 10^{-14} m^2. As mentioned above, in our previous work[15], a high-permeability porous membrane was manufactured on the conventional filter substrate using fine alumina particles. The permeability was estimated as 7.7 x 10^{-14} m^2 with a porosity of 94.3%. Since the density of TWC-particles is higher than that of alumina-particles, it is not easy to increase the porosity even under the condition of smaller TWC-particle. Consequently, a high permeability TWC-particles membrane filter can be manufactured by a range of particle size around 1~ 2 μm which should be completely suspended in flowing gas.

4. Conclusion

In the TWC-particles membrane manufacturing process, a similar analogical percolation structure is obtained under the conditions of the particle sizes of 0.5, 0.93 and 1.2 μm and the superficial velocities of 5, 25 and 50 mm/s. The porosity of the TWC-particles membrane filter can be estimated by using infiltration of the epoxy resin into the micrometer-sized pores and then by making the comparison between the cross-sectional areas of TWC-particles and the resin. The porosity of the TWC-particle membrane layer is around 64 % (61.8 ~ 67 %). The permeability of the TWC-particles membrane layer with the particle size of 1.2 μm becomes highest and the value is estimated as 1.23 x 10^{-14} m^2. The permeability depends strongly on the TWC-particle size since the porosity is not increase drastically with decreasing particle size in this study.

Acknowledgement

The author(s) would like to express their gratitude to the New Energy and Industrial Technology Development Organization (NEDO), Research Association of Automotive Internal Combustion Engines (AICE) in Japan for the support, and the staffs from Open Facility Center at Ookayama Campus, Tokyo Tech for their technical support.

References

(1) Dong, R., Zhang, Z., Ye, Y., Huang, H., Cao, C., Review of Particulate Filters for Internal Combustion Engines, Processes, 993 (10), p. 1-27, 2022, https://doi.org/10.3390/pr10050993
(2) Kittelson, D. B., Engines and Nanoparticles: A Review, Journal of Aerosol Science, 29 (5/6), p. 575-588, 1998, https://doi.org/10.1016/S0021-8502(97)10037-4
(3) Joshi, A., Johnson, T. V., Gasoline Particulate Filters – A Review, Emission Control Science and Technology, 4, p. 219-239, 2018, https://doi.org/10.1016/S0021-8502(97)10037-4
(4) Chincholkar, S. P., Suryawanshi, J. G., Gasoline Direct Injection: An Efficient Technology, Energy Procedia, 90, p. 666-672, 2016, https://doi.org/10.1016/j.egypro.2016.11.235
(5) Saliba, G., Saleh, R., Zhao, Y., Presto, A. A., Lambe, A. T., Frodin, B. et al., Comparison of Gasoline Direct-Injection (GDI) and Port Fuel Injection (PFI) Vehicle Emissions: Emission Certification Standards, Cold-Start, Secondary Organic Aerosol Formation Potential, and Potential Climate Impacts, Environmental Science and Technology, 51 (11), p. 6542-6552, 2017, https://doi.org/10.1021/acs.est.6b06509
(6) Duronio, F., Vita, A. D., Montanaro, A., Villante, C., Gasoline Direct Injection Engines – A Review of Latest Technologies and Trends. Part 2, Fuel, 265, p. 116947-116955, 2020, https://doi.org/10.1016/j.fuel.2019.116947
(7) Qian, Y., Li, Z., Yu, L., Wang, X., Lu, X., Review of the State-of-the-art of Particulate Matter Emissions from Modern Gasoline Fueled Engines, Applied Energy, 238, p. 1269-1298, 2019, https://doi.org/10.1016/j.apenergy.2019.01.179
(8) Twigg, M. V., Catalytic Control of Emissions from Cars, Catalysis Today, 163, p. 33-41, 2011, https://doi.org/10.1016/j.cattod.2010.12.044
(9) Montini, T., Melchionna, M., Monai, M., Fornasiero, P., Fundamentals and Catalytic Applications of CeO_2-Based Materials, Chemical Reviews, 116 (10), p. 5987-6041, 2016, https://doi.org/10.1021/acs.chemrev.5b00603
(10) Xia, W., Zheng, Y., He, X., Yang, D., Shao, H., Remias, J., Catalyzed Gasoline Particulate Filter (GPF) Performance: Effect of Driving Cycle, Fuel, Catalyst Coating, SAE Technical Paper2017-01-2366, 2017, https://doi.org/10.4271/2017-01-2366
(11) Richter, J. M., Klingmann, R., Spiess, S., Wong, K., Application of Catalyzed Gasoline Particulate Filters to GDI Vehicles, SAE International Journal of Engines, 5 (3), p.1361-1370, 2012, https://doi.org/10.4271/2012-01-1244
(12) Karin, P., Hanamura, K., Microscopic Visualization of Particulate Matter Trapping and Oxidation Behaviors in a Diesel Particulate Catalyst-Membrane Filter, JSAE Annual Congress Research Paper, 41 (4), p.853-858, 2010, https://doi.org/10.11351/jsaeronbun.41.853
(13) Sanui, R., Hanamura, K., Electron Microscopic Time-lapse Visualization of Surface Pore Filtration on Particulate Matter Trapping Process, Journal of Microscopy, 263, p. 1-9, 2016, https://doi.org/10.1111/jmi.12386
(14) R. Sanui, K. Hanamura. Scanning electron microscopic visualization of bridge formation inside the porous channels of diesel particulate filters, SAE International Journal of Fuels Lubricants. 9 (3), p. 725-733, 2016.
(15) Nakajima, S., Sanui, R., Hanamura, K., Soot Trapping by High-permeability Porous Membrane Filter Made of Aggregates of Alumina Nanoparticles, International Journal of Automotive Engineering, 8 (3), p. 105-111, 2017, https://doi.org/10.20485/jsaeijae.8.3_105

(16) Suteerapongpun, T., Kitagawa, Y., Srilomsak, M., Hanamura, K., Development of Membrane Filter Made of Alumina and Silver-Palladium Particles for High-Filtration Efficiency, Low-pressure Drop and Low-Soot Oxidation Temperature, International Journal of Automotive Engineering, 11 (4), p. 151-158, 2020, https://doi.org/10.20485/jsaeijae.11.4_151
(17) Hanamura, K., Inaba, M., Kawabe, K., and Mitarai, K., Oxidation Enhancement of Particulate Matters Deposited on Catalyzed Membrane Filter by Nitrogen Oxides Diffusion, Transactions of Society of Automotive Engineers of Japan, 53(1), p. 100-106, 2022.
(18) Koko, P., Suteerapongpun, T., Hanamura, K., Manufacturing of Three-way Catalyst Membrane Particulate Filter and Porosity Measurement using Electron Microscopy Image Analysis, 2022 JSAE Annual Congress (Spring), Society of Automotive Engineering of Japan, JSAE 2022502, Yokohama, Japan, May. 25-27, 2022.
(19) Kuwabara, S., The forces Experienced by Randomly Distributed Parallel Circular Cylinders or Spheres in a Viscous Flow at Small Reynolds Numbers, Journal of the Physical Society of Japan, 14 (4), p. 527-532, 1958. https://doi.org/10.1143/JPSJ.14.527